Evidence for the extinction of the $N = 20$ neutron-shell closure for ^{32}Mg from direct mass measurements

A. Chaudhuri,[1,*] C. Andreoiu,[2] T. Brunner,[1,3] U. Chowdhury,[1,4] S. Ettenauer,[1,5,†] A. T. Gallant,[1,5] G. Gwinner,[4]
A. A. Kwiatkowski,[1] A. Lennarz,[1,6] D. Lunney,[7] T. D. Macdonald,[1,5] B. E. Schultz,[1] M. C. Simon,[1,‡]
V. V. Simon,[1,8,§] and J. Dilling[1,5]

[1]*TRIUMF, 4004 Wesbrook Mall, Vancouver, British Columbia V6T 2A3, Canada*
[2]*Department of Chemistry, Simon Fraser University, Burnaby, British Columbia V5A 1S6, Canada*
[3]*Department of Physics, Stanford University, Stanford, California 94305, USA*
[4]*Department of Physics and Astronomy, University of Manitoba, Winnipeg, Manitoba R3T 2N2, Canada*
[5]*Department of Physics and Astronomy, University of British Columbia, Vancouver, British Columbia V6T 1Z1, Canada*
[6]*Institut für Kernphysik, Westfälische Wilhelms-Universität, 48149 Münster, Germany*
[7]*CSNSM-IN2P3-CNRS, Université de Paris Sud, 91405 Orsay, France*
[8]*Max-Planck-Institut für Kernphysik, 69117 Heidelberg, Germany*

The "island of inversion" around ^{32}Mg is one of the most important paradigms for studying the disappearance of the stabilizing "magicity" of a shell closure. We present the first Penning-trap mass measurements of the exotic nuclides $^{29-31}$Na and $^{30-34}$Mg, which allow precise determination of the empirical shell gap for ^{32}Mg. The new value of 1.10(3) MeV is the smallest observed shell gap for any nuclide with a canonical magic number.

PACS number(s): 21.10.Dr, 21.60.Cs, 27.30.+t

I. INTRODUCTION

The nuclear shell model [1] provides the foundation of our understanding of the atomic nucleus. The most salient feature of the shell model is the existence of magic numbers of neutrons or protons corresponding to closed shells that form nuclides of exceptional stability and spherical shape. The strength of a nuclear shell closure is indicated by the energy gap between the closed shell and the next available orbital. Exceptionally strong shell closures laid the foundation for the nuclear shell model discovered with stable nuclides, but these magic numbers have shown an elusive character with radioactive nuclides. For these unstable nuclides, known magic numbers can vanish, and new ones have appeared [2,3].

The case of $N = 20$ is a crucial benchmark for the disappearance of the stabilizing effects of closed shells. Anomalies in the nuclear structure in the region around the neutron magic number $N = 20$ for $A \approx 32$ have been experimentally known for many years [4,5]. The first indications of the breakdown of the $N = 20$ shell closure were revealed from the online mass spectrometry studies of Na ($Z = 11$) across the $N = 20$ shell closure [4]. The masses of ^{31}Na and ^{32}Na obtained from Ref. [4] implied that $N = 20$ isotones neighboring ^{32}Mg are more tightly bound than expected from the standard shell model predictions. The breakdown of the $N = 20$ shell closure in this region originates in nuclear deformation and the resultant inversion of the standard sd-shell configuration

and pf-shell intruder configuration, which has led to this region in the nuclear chart being known as the "island of inversion" [6]. Here the intruder states imply the states composed of shell-model configurations with $1p1h$, $2p2h$, or higher excited configurations across the $N = 20$ shell gap [7].

Immediately following the first conventional mass measurements, nuclear decay spectroscopy offered more evidence of an unexpected onset of deformation near $N = 20$ [5]. Coulomb excitation studies of ^{32}Mg also confirmed the large deformation and pointed to the vanishing of the $N = 20$ shell gap [8]. Spectroscopic measurements continued to provide important information about the extent of the island of inversion [9,10]. Measurement of the spin and magnetic moment of ^{31}Mg [11] and ^{33}Mg [12] by laser and β-NMR spectroscopy played a key role in understanding of the island of inversion. Developments with radioactive beams have added to the wealth of experimental data and now allow precise probing of different levels by selective reactions, as illustrated by the discovery of a deformed 0^+ state in ^{32}Mg from a transfer reaction [13].

On the theoretical side, the change in the shell structure at $N = 20$ is now largely attributed to the monopole effect of tensor forces [14,15]. In this picture, the reduced attraction of the proton $d_{5/2}$ orbital towards the dripline allows the neutron $d_{3/2}$ orbital to increase in energy, reducing the gap to the $f_{7/2}$. As a consequence, a new gap arises with respect to the $s_{1/2}$ orbital for $N = 16$, confirmed by the recent results showing the double magicity of ^{24}O [2,3].

Direct mass measurements allow the empirical determination of the strength of a nuclear shell closure. Such a shell gap, while using information about neighboring nuclides, is an experimental observable. Penning traps confine charged particles to a small volume with well-defined electric and magnetic fields, making them the tool of choice for high-accuracy and high-precision mass measurements of radioactive isotopes. For this reason, several Penning-trap mass spectrometers

---

*ankur@triumf.ca

†Present address: Department of Physics, Harvard University, Cambridge, Massachusetts 02138, USA.

‡Present address: Stefan Meyer Institute for Subatomic Physics, Austrian Academy of Sciences, Boltzmanngasse 3, 1090 Vienna, Austria.

§Present address: Helmholtz-Institut Mainz, 55128 Mainz, Germany.

054317-1

have been installed at radioactive ion beam (RIB) facilities worldwide [16]. In particular, the beam production, advanced ion manipulation, and mass measurement must be compatible with the decay lifetime of the radioactive ions, here 17–313 ms. With the TRIUMF's Ion Trap for Atomic and Nuclear science (TITAN) experiment [17], Penning-trap mass spectrometry has developed to the point where precision mass measurements of exotic short-lived species ($t_{1/2} \sim 10$–50 ms) can now achieve a new level of precision and accuracy for the binding energy [18]. In this article we report the first Penning-trap results on the island-of-inversion nuclides $^{29-31}$Na and $^{30-34}$Mg employing the TITAN spectrometer.

II. EXPERIMENTAL DETAILS AND RESULTS

The TITAN Penning-trap mass spectrometer is coupled to the rare-isotope-beam facility Isotope Separator and Accelerator (ISAC) [19] at TRIUMF. The TITAN facility consists of three ion traps: a gas-filled radiofrequency quadrupole ion trap (RFQ) [20] for cooling and bunching of ions, an electron beam ion trap (EBIT) [21] for charge breeding [22], and a precision Penning trap for the mass measurements. The short-lived nuclides studied here were produced for the first time by impinging a 10-μA proton beam on a UC$_2$ target and employing a resonant laser ionization scheme [23] at ISAC. The yield varied from $\approx 10^6$ particles per second for ^{30}Mg to $\approx 10^3$ particles per second for more exotic ^{34}Mg. Radioactive ion beams delivered by ISAC at energy ≈ 20 keV were injected into the RFQ cooler and buncher, where the ions were cooled, and then ejected as a low-emittance, bunched beam. Due to the short half-lives, the singly charged ions extracted from the RFQ were sent to the Penning trap for the mass measurements, bypassing the EBIT.

In Penning-trap mass spectrometry, the atomic mass is determined from the measurement of the ion cyclotron frequency

$$\nu_c = \frac{1}{2\pi} \left(\frac{q}{m_{\text{ion}}} \right) B, \quad (1)$$

where B is the magnetic field strength, q is the charge, and m_{ion} is the mass of the ion. The cyclotron frequency of the trapped ion was measured by the time-of-flight ion-cyclotron-resonance (TOF-ICR) detection method [24]. TOF resonances of ^{31}Na$^+$, ^{32}Mg$^+$, and ^{34}Mg$^+$ are shown in Fig. 1. To calibrate the magnetic field, ν_c of the ion of interest is compared to the $\nu_{c,\text{ref}}$ of a reference ion with a well-known mass m_{ref}, i.e.,

$$\frac{m_{\text{ref}}}{m_{\text{ion}}} = \left(\frac{\nu_c}{\nu_{c,\text{ref}}} \right) \left(\frac{q_{\text{ref}}}{q} \right) = r \left(\frac{q_{\text{ref}}}{q} \right). \quad (2)$$

Here $r = \frac{\nu_c}{\nu_{c,\text{ref}}}$ is the cyclotron frequency ratio. A count-rate class analysis [25] was carried out for all frequency measurements to account for possible systematic shifts in the cyclotron frequency and exclude the influences of any contaminant ion species in the Penning trap.

Either ^{39}K$^+$ ($\delta M \approx 5$ eV/c^2) ions obtained from a surface ion source coupled to TITAN or ^{16}O$_2^+$ ($\delta M \approx 0.3$ eV/c^2) ions obtained from the ISAC off-line ion source OLIS [26] were used as reference ions during the measurements (where δM is
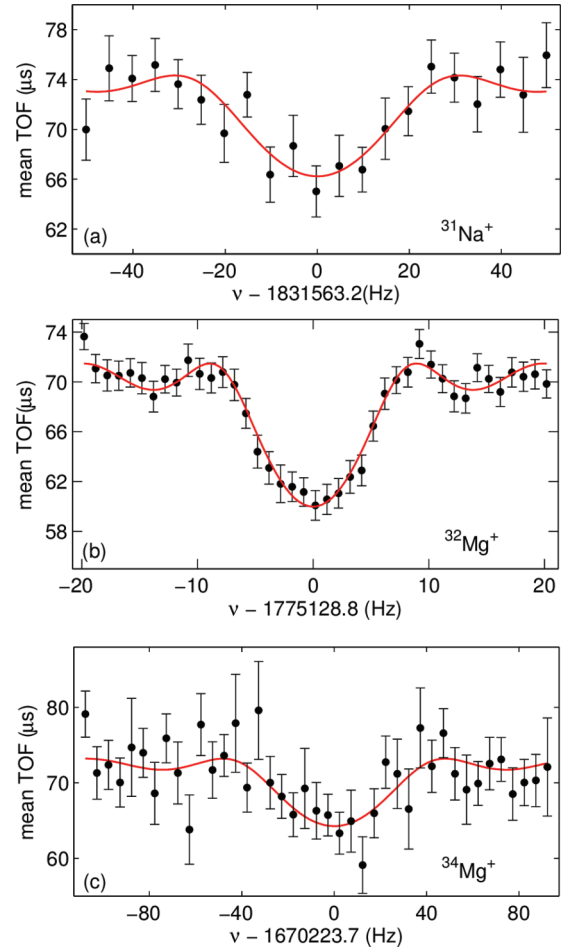

FIG. 1. (Color online) Time-of-flight (TOF) ion-cyclotron resonances for (a) ^{31}Na$^+$ ($t_{1/2} = 17$ ms), (b) ^{32}Mg$^+$ ($t_{1/2} = 86$ ms), and (c) ^{34}Mg$^+$ ($t_{1/2} = 20$ ms) ions. The TOF is shown as a function of the excitation frequency for excitation times of 28, 97, and 18 ms, respectively, applied in the TITAN Penning trap. The solid line represents a fit of the theoretically expected resonance curve [24] to the data points. The centroid corresponds to the cyclotron frequency, from which the mass is deduced.

the uncertainty of the atomic mass taken from the 2012 atomic mass evaluation (AME) [27]). The atomic mass M of each short-lived nuclide was calculated from its measured frequency ratio r and the reference ion's mass and was corrected for the electron mass. The electron binding energy of less than 10 eV was neglected for the present measurements, whose statistical mass uncertainties are above 1 keV. The measurement results are summarized in Table I in terms of the mass excess $= M - A$ in keV/c^2 where M is the atomic mass and A is the atomic mass number in atomic mass units (u) taken from the 2010 Committee on Data for Science and Technology (CODATA)-recommended values [32]. Since the reference mass values can change in the future, the measured frequency ratio r is listed in Table I.

Large deviations were found in the mass excess values from past measurements as shown in Table I and illustrated in Fig. 2. The time-of-flight measurements used in the past were prone to systematic errors due to the complex calibration and error

TABLE I. Summary of the results of the TITAN mass measurements of $^{29-31}$Na and $^{30-34}$Mg. The mass excess ME with one-standard-deviation uncertainty is compared with the ME from AME2003 [28], post-AME 2003 experiments [29,30], AME2011 [31], and AME2012 [27]. Note that the given uncertainties in parentheses are the total uncertainties. The sources of the post-AME2003 experiments are cited in brackets. Note the AME2012 entries are dominated by the present TITAN measurements.

Nuclide	$T_{1/2}$ (ms)	Reference	r	ME_{TITAN} (keV/c^2)	ME_{AME2003} (keV/c^2)	ME_{expt} (keV/c^2)		ME_{AME2011} (keV/c^2)	ME_{AME2012} (keV/c^2)
^{29}Na$^+$	44.1	^{39}K$^+$	1.34344900(46)	2686.0(9.3)	2665(13)	2669(12)	[29]	2670(12)	2680(7)
^{30}Na$^+$	48.4	^{39}K$^+$	1.29840205(52)	8471.7(11.3)					
^{30}Na$^+$	48.4	^{16}O$_2^+$	1.06600554(20)	8475.4(5.2)					
^{30}Na$^+$	48.4			8474.8(4.7)[a]	8361(25)	8375(23)	[29]	8374(23)	8475(5)
^{31}Na$^+$	17.0	^{39}K$^+$	1.2563648(10)	12261(23)	12650(210)	12520(110)	[30]	12540(103)	12261(23)
^{30}Mg$^+$	313	^{16}O$_2^+$	1.06666796(13)	$-8883.8(3.4)$	$-8911(8)$	$-8892(13)$	[29]	$-8892(13)$	$-8884(3)$
^{31}Mg$^+$	232	^{16}O$_2^+$	1.03204213(11)	$-3122.3(3.0)$	$-3217(12)$	$-3190(16)$	[29]	$-3190(17)$	$-3122(3)$
^{32}Mg$^+$	86	^{16}O$_2^+$	0.99970996(11)	$-828.8(3.1)$	$-955(18)$	$-915(20)$	[29]	$-912(18)$	$-829(3)$
^{33}Mg$^+$	90.5	^{16}O$_2^+$	0.96923179(9)	4962.2(2.8)	4894(20)	4947(22)	[29]	4947(22)	4962.2(2.9)
^{34}Mg$^+$	20	^{16}O$_2^+$	0.94062917(87)	8323(29)	8810(230)	8560(90)	[30]	8560(90)	8323(29)

[a]Weighted average of mass excesses obtained from two independent experiments using ^{39}K$^+$ and ^{16}O$_2^+$ as reference ions respectively.

evaluation technique. Often they used calibrants far from the stable region of the nuclear chart, hence re-evaluation was needed when the reference masses changed. The TITAN mass values also represent significant improvement in the resulting precision.

III. DISCUSSION

The two-nucleon separation energy, an important quantity for probing the evolution of shell closures, is derived from the experimental mass data. The two-neutron separation energy

$$S_{2n}(Z, N) = B(Z, N) - B(Z, N - 2)$$
$$= -M(Z, N) + M(Z, N - 2) + 2m_n, \quad (3)$$

where $B(Z, N)$ is the binding energy, $M(Z, N)$ is the atomic mass, and m_n is the neutron mass, is a key measure of how tightly valence neutrons are bound to the nucleus and hence is sensitive to the neutron-shell closure. The relative strength of the difference in binding energies before and after a purported shell closure can be quantified by an empirical shell gap, as defined by [33]

$$\Delta_n(Z, N) = S_{2n}(Z, N) - S_{2n}(Z, N + 2). \quad (4)$$

The empirical shell gap $\Delta_n(Z, N)$ is a sensitive probe to the relative enhancement in binding energy found in magic nuclides and is directly determined from mass measurements. Note that the empirical shell gap does not represent the energy difference between effective single-particle energies, a signature of shell evolution that is model dependent. As a double derivative, $\Delta_n(Z, N)$ involves the masses of three nuclides as seen from Eqs. (3) and (4), requiring high measurement precision to minimize its uncertainty. The masses of ^{30,32,34}Mg and ^{29,31,33}Na are needed for the evaluation of the empirical shell gap for ^{32}Mg and ^{31}Na, respectively. The uncertainties associated with earlier conventional mass measurements [29–31] were too large (see Fig. 2) for a reliable determination of the empirical shell gap.

The new S_{2n} values for Mg and Na isotopes are plotted in Fig. 3 and are compared with AME2003 [28] and AME2011 [31]. We compare to AME2011 rather than the new AME2012 [27] because the present TITAN mass measurements are included in the AME2012 (see Table I). Note that in addition to the present TITAN mass values, the mass values of ^{28,29,35,36}Mg, and ^{27,28,32}Na from AME2012 and that of ^{33}Na from the recent experiments [30,34] were used to determine the new S_{2n} values.

The new mass values provide information relevant to the breakdown of the established nuclear shell model in the vicinity of ^{32}Mg. The empirical shell gap Δ_n for ^{32}Mg ($Z = 12, N = 20$) was determined using the atomic masses of ^{30,32,34}Mg reported here. The value obtained is only 1.10(3) MeV, which reveals the lowest observed strength of nuclear shell closure for a nuclide with a conventional magic number. The present measurements of ^{29,31}Na improve the precision of Δ_n for ^{31}Na ($Z = 11, N = 20$). The Δ_n for ^{31}Na was calculated to be 1.79(23) MeV.
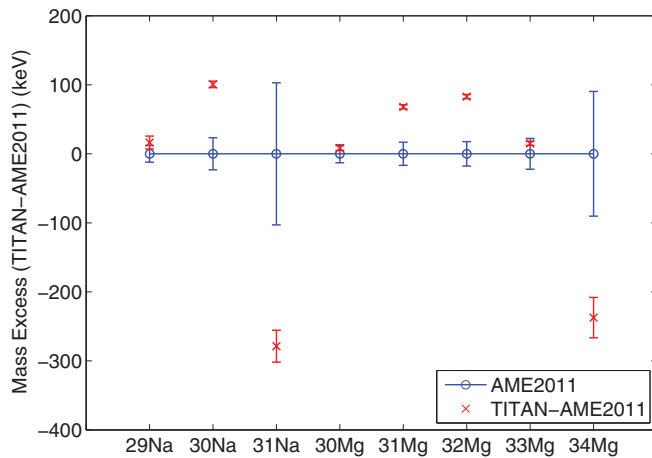

FIG. 2. (Color online) Comparison of the mass excess from the present work to the values from AME2011 [31]. The present TITAN mass measurements are already included in the new AME2012 [27].
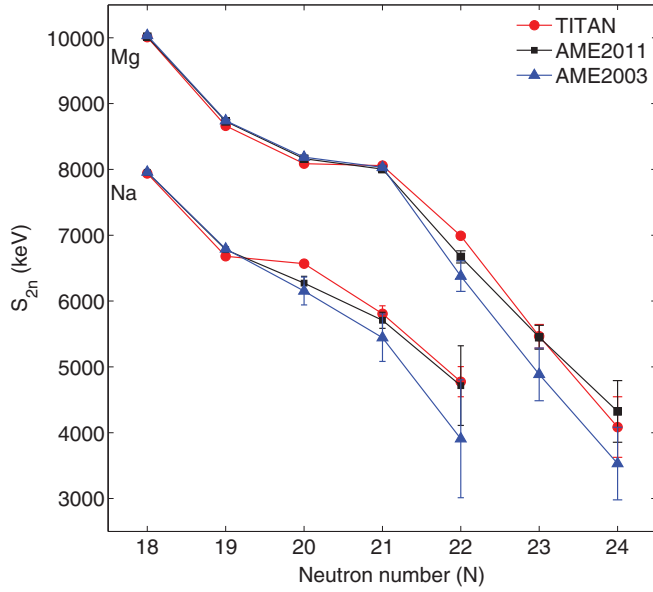
FIG. 3. (Color online) Two-neutron separation energy S_{2n} plots of Mg and Na isotopes. The solid circles represent the S_{2n} values determined from the present work. The squares and the triangles denote S_{2n} values from AME2011 [31] and AME2003 [28], respectively.

Figure 4 displays a comparison of the empirical shell gap Δ_n from $Z = 10$ to 22 for the magic number $N = 20$. Enhanced stability demonstrated by an exceptionally high Δ_n value can be seen for doubly magic ^{40}Ca ($Z = N = 20$) due to additional like-nucleon pairing. A significant drop of shell strength below $Z = 14$ reveals the presence of the island of inversion. The empirical shell gap Δ_n using the mass values from AME2011 shows the trend of the $N = 20$ shell closure; however, due to the large uncertainty it was impossible to come to any conclusion about the shell quenching. The small empirical shell gap obtained from the first Penning-trap measurements around ^{32}Mg using the TITAN experimental setup is consistent with known deformation which leads to increased binding energy.

We compare our results (Fig. 4) with the Hartree-Fock-Bogoliubov mass model (HFB21) using nonconventional Skyrme forces [35]. The mean-field model HFB21 yields $\Delta_n(^{32}$Mg$) = 0.46$ MeV; however, this model predicts ^{32}Mg to be spherical in contrast to the experimentally determined shape [8,11]. We also compare our results with other theoretical studies: the angular-momentum projected generator-coordinate method with the Skyrme interaction SLy4 (GCM + SLy4) [36] which predicts $\Delta_n(^{32}$Mg$) = 1.82$ MeV, and the Monte Carlo shell model (MCSM) based on the quantum Monte Carlo diagonalization method [37] which predicted $\Delta_n(^{32}$Mg$) = 1.8$ MeV. The conventional shell model calculation [38], which is limited by the current knowledge of the interaction, predicted $\Delta_n(^{32}$Mg$)$ to be negative. Despite the large differences in the Δ_n value, the standard shell model studies give a description of the anomaly which indicates the breaking of the shell closure at $N = 20$. The $N = 20$ region is challenging for energy-density functional methods [39], as it involves light nuclei, and also for *ab initio* methods, which have not been able to access the island of inversion to date.
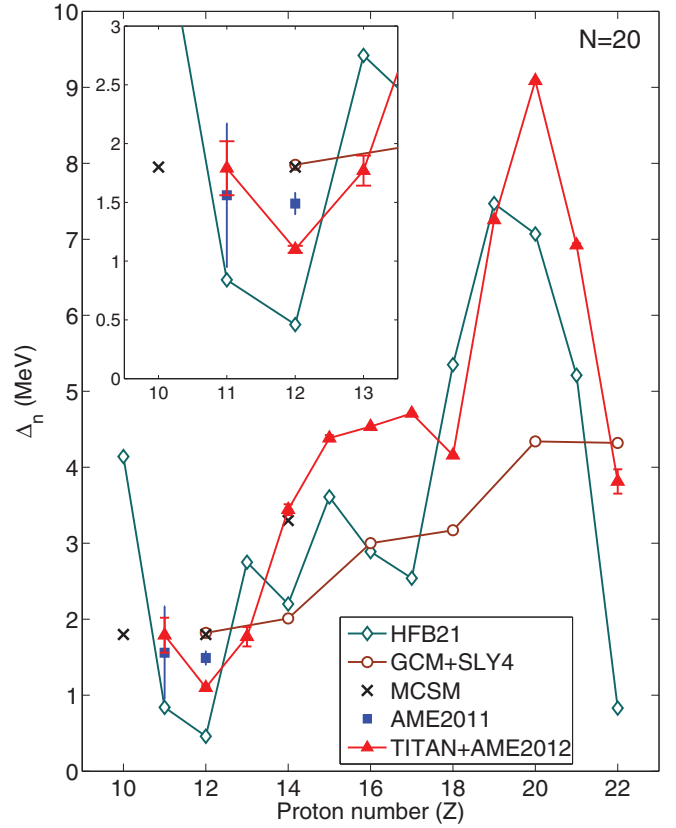

FIG. 4. (Color online) Comparison of experimental and theoretical empirical neutron shell gap Δ_n for nuclides with magic neutron number $N = 20$. The solid triangles represent the experimentally obtained values from TITAN and AME2012. The TITAN measurements contribute to the cases of ^{32}Mg ($Z = 12$, $N = 20$) and ^{31}Na ($Z = 11$, $N = 20$). The Δ_n values obtained from HFB21, the angular-momentum projected generator method with the Skyrme interaction SLy4 (GCM + SLy4), and the Monte Carlo shell model (MCSM) are shown as open diamonds, open circles, and crosses respectively. The Δ_n values of ^{32}Mg and ^{31}Na from AME2011 are shown as solid rectangles for comparison. Δ_n for $Z = 10$ to 13 are shown in the inset.

The results from HFB21 and SLy4, while both based on the mean-field approach, complement each other. The parameters of the HFB21 interaction are fit to the entire mass table, resulting in a better overall fit to the shell gap values. The parameters of the SLy4 interaction are adjusted to a restricted set of (doubly magic) nuclides. Both models give similar extrapolations for the $N = 50$ and $N = 82$ shell closures and the tendency is the same for $N = 20$. (Unfortunately there are no SLy4 predictions for $Z < 12$.)

There is discussion in literature (e.g., Ref. [40]) considering the validity of the definition of the empirical shell gap given by Eq. (4). In principle this definition should apply only to spherical nuclides, which we know ^{32}Mg is not. Moreover, the shell gap defined this way reflects contributions from three different nuclides, spanning five neutron numbers. The definition using S_n reduces the range to three neutron numbers but introduces the effect of pairing, but it is important to recall that Δ_n has the merit of being derived from experimental observables—unlike

the effective single-particle energy, which is a theoretical quantity. Although it cannot be claimed that Δ_n is a benchmark for determining the shell gap strength, the use of Δ_n does offer a benchmark for comparisons with the theoretical mass differences.

The found 1.1-MeV empirical shell gap is interesting in itself. The $N = 20$ shell closure, so strong for $Z = 20$, is extinguished for $Z = 12$, reduced in strength by one order of magnitude. Given the higher value for $Z = 11$, it is possible to think that the shell gap may continue its increase, rising for $Z = 10$ through the (unbound) $Z = 8$.

Any theory correctly describing the magicity of the $N = 20$ closure for $Z > 13$ must also predict the binding energy differences for those Z where the empirical shell gap is very small. The mechanism of the tensor force provides an insightful qualitative picture. Although quantitative mass predictions were provided by Refs. [38,41] over 10 years ago, no new calculations have appeared since. The corresponding spectroscopic calculations also severely underestimated the 0^+ state reported in Ref. [12]. Moreover, the reaction codes

used in that work required an adjustment to the binding energy of ^{32}Mg. Recent success with three-body forces from chiral effective field theory [42,43] show promise for accurate S_{2n} predictions. We eagerly await such calculations for the island of inversion.

[1] M. Goeppert Mayer, *The Shell Model*, Nobel Lectures, Physics 1963–1970 (Elsevier, Amsterdam, the Netherlands, 1972).

[2] R. Kanungo *et al.*, Phys. Rev. Lett. **102**, 152501 (2009).

[3] C. R. Hoffman *et al.*, Phys. Lett. B **672**, 17 (2009).

[4] C. Thibault *et al.*, Phys. Rev. C **12**, 644 (1975).

[5] C. Détraz *et al.*, Phys. Rev. C **19**, 164 (1979).

[6] E. K. Warburton, J. A. Becker, and B. A. Brown, Phys. Rev. C **41**, 1147 (1990).

[7] Y. Utsuno, T. Otsuka, T. Glasmacher, T. Mizusaki, and M. Honma, Phys. Rev. C **70**, 044307 (2004).

[8] T. Motobayashi *et al.*, Phys. Lett. B **346**, 9 (1995).

[9] P. Doornenbal *et al.*, Phys. Rev. Lett. **103**, 032501 (2009).

[10] G. Christian *et al.*, Phys. Rev. Lett. **108**, 032501 (2012).

[11] G. Neyens *et al.*, Phys. Rev. Lett. **94**, 022501 (2005).

[12] D. T. Yordanov *et al.*, Phys. Rev. Lett. **99**, 212501 (2007).

[13] K. Wimmer *et al.*, Phys. Rev. Lett. **105**, 252501 (2010).

[14] T. Otsuka, R. Fujimoto, Y. Utsuno, B.A. Brown, M. Honma, and T. Mizusaki, Phys. Rev. Lett. **87**, 082502 (2001).

[15] T. Otsuka, T. Suzuki, M. Honma, Y. Utsuno, N. Tsunoda, K. Tsukiyama, and M. Hjorth-Jensen, Phys. Rev. Lett. **104**, 012501 (2010).

[16] K. Blaum, J. Dilling, and W. Nörtershäuser, Phys. Scr. T **152**, 014017 (2013).

[17] J. Dilling *et al.*, Int. J. Mass Spectrom. **251**, 198 (2006).

[18] A. Chaudhuri *et al.*, Appl. Phys. B (2013), doi: 10.1007/s00340-013-5618-8.

[19] M. Dombsky *et al.*, Rev. Sci. Instrum. **71**, 978 (2000).

[20] T. Brunner *et al.*, Nucl. Instrum. Methods Phys. Res. Sect. A **676**, 32 (2012).

[21] A. Lapierre *et al.*, Nucl. Instrum. Methods Phys. Res. Sect. A **624**, 54 (2010).

[22] S. Ettenauer *et al.*, Phys. Rev. Lett. **107**, 272501 (2011).

[23] J. Lassen *et al.*, in *Proceedings of the Sixth International Workshop on Application of Lasers in Atomic Nuclei Research (LASER 2004)*, edited by Z. Blaszczak, B. Markov, and K. Marinova (Springer, Berlin, 2006), pp. 69–75.

[24] M. König *et al.*, Int. J. Mass Spectrom. **142**, 95 (1995).

[25] A. Kellerbauer *et al.*, Eur. Phys. J. D **22**, 53 (2003).

[26] K. Jayamanna *et al.*, Rev. Sci. Instrum. **67**, 1061 (1996).

[27] M. Wang *et al.*, Chin. Phys. C **36**, 1603 (2012).

[28] G. Audi, A. H. Wapstra, and C. Thibault, Nucl. Phys. A **729**, 337 (2003).

[29] C. Gaulard *et al.*, Nucl. Phys. A **766**, 52 (2006).

[30] B. Jurado *et al.*, Phys. Lett. B **649**, 43 (2007).

[31] G. Audi and W. Meng (private communication) [http://amdc.in2p3.fr/bulletins/amdc.114].

[32] CODATA Internationally Recommended Values of the Fundamental Physical Constants [http://physics.nist.gov/constants]

[33] D. Lunney *et al.*, Rev. Mod. Phys. **75**, 1021 (2003).

[34] L. Gaudefroy *et al.*, Phys. Rev. Lett. **109**, 202503 (2012).

[35] S. Goriely, N. Chamel, and J. M. Pearson, Phy. Rev. C **82**, 035804 (2010).

[36] M. Bender, G. F. Bertsch, and P.-H. Heenen, Phy. Rev. C **78**, 054312 (2008).

[37] Y. Utsuno, T. Otsuka, T. Mizusaki, and M. Honma, Phy. Rev. C **60**, 054315 (1999).

[38] E. Caurier, F. Nowacki, A. Poves, and J. Retamosa, Phy. Rev. C **58**, 2033 (1998).

[39] J. Erler *et al.*, Nature (London) **486**, 509 (2012).

[40] M.-G. Porquet and O. Sorlin, Phy. Rev. C **85**, 014307 (2012).

[41] R. Rodríguez-Guzmán, J. L. Egido, L. M. Robledo *et al.*, Nucl. Phys. A **709**, 201 (2002).

[42] A. T. Gallant *et al.*, Phys. Rev. Lett. **109**, 032506 (2012).

[43] F. Wienholtz *et al.*, Nature (London) **498**, 346 (2013).